J MATER SCI 41 (2006) 2587–2595

Nanostructural characterization of YBCO films on metal tape with textured buffer layer fabricated by pulsed-laser deposition

T. KATO*, H. SASAKI, Y. SASAKI, T. HIRAYAMA, Y. IKUHARA
Materials R&D Lab, Japan Fine Ceramics Center, 2-4-1 Mutsuno, Atsuta-ku, Nagoya 456-8587, Japan
E-mail: tkato@jfcc.or.jp

T. WATANABE, A. IBI, H. IWAI, T. MUROGA, S. MIYATA, Y. YAMADA
SRL-Nagoya Coated Conductor Center, ISTEC, 2-4-1 Mutsuno, Atsuta-ku, Nagoya 456-8587, Japan

Y. IIJIMA, K. KAKIMOTO, Y. SUTOH, T. SAITOH
Material Technology Lab, Fujikura Ltd., 1-5-1 Kiba, Koto-ku, Tokyo 135-8512, Japan

T. IZUMI
SRL-Division of Superconducting Tapes and Wires, ISTEC, 1-10-13 Shinonome, Koto-ku, Tokyo 135-0062, Japan

Y. SHIOHARA
SRL-Nagoya Coated Conductor Center, ISTEC, 2-4-1 Mutsuno, Atsuta-ku, Nagoya 456-8587, Japan; SRL-Division of Superconducting Tapes and Wires, ISTEC, 1-10-13 Shinonome, Koto-ku, Tokyo 135-0062, Japan

Published online: 17 April 2006

Thick $YBa_2Cu_3O_{7-x}$ (YBCO) films with high critical current density (J_c) values were deposited by pulsed-laser deposition (PLD) on Hastelloy with a textured $CeO_2/Gd_2Zr_2O_7$ buffer layer. Both cross-sectional and plan-view TEM specimens of the YBCO films were prepared, and then the nanostructural characterization of the films was performed by transmission electron microscopy (TEM). The YBCO films less than 1 μm thick were predominantly composed of *c*-axis-oriented grains, however, many *a*-axis-oriented grains, which grew larger with the increase of the thickness of the YBCO film, were formed beyond about 1 μm from the CeO_2 interface. We found Y_2O_3 and copper oxides between *a*- and *c*-axes-oriented grains. In particular, Y_2O_3 grains were formed between the {001} plane of an *a*-axis-oriented grain and the {100} or {010} plane of a *c*-axis-oriented grain. The orientation relationships between Y_2O_3 and YBCO are found to be; (001)YBCO//(001)Y_2O_3 and (100)YBCO//(110)Y_2O_3. In addition, we also found gaps between YBCO grains. Since *a*-axis-oriented grain growth and the formation of Y_2O_3, copper oxides and the gaps are considered to reduce the J_c values of the YBCO film, it is important to determine the optimum process conditions to suppress the nucleation of *a*-axis-oriented grains, impurity oxides and gaps.

*Author to whom all correspondence should be addressed.

0022-2461 © 2006 Springer Science + Business Media, Inc.
DOI: 10.1007/s10853-006-7785-z

1. Introduction

In recent years, a great deal of research worldwide has been directed towards developing $YBa_2Cu_3O_{7-x}$ (YBCO) coated superconductor tapes. In order to fabricate YBCO films with high critical current density (J_c) values, it is important to achieve highly and biaxially textured YBCO films since highly oriented texturing is crucial in carrying high electric current in superconducting states. To form such YBCO films on a metal tape, the use of biaxially textured ceramics buffer layers is necessary. Several methods have been used to coat biaxially textured ceramics on metal tapes and several materials have been tested as template materials for YBCO layers. In particular ion-beam-assisted deposition (IBAD) can deposit biaxially textured ceramics layers on a non-textured metal tape [1–7]. Iijima *et al.* found that the time required to form Gd–Zr-oxide (GZO) films with sufficient biaxial orientation on the metal tapes by IBAD is shorter than any other pyrochlore- or fluorite-type crystals [4, 5]. In addition, Muroga *et al.* formed CeO_2 films with in-plane alignment ($\Delta\phi$), measured by X-ray pole figure, less than 5 degrees on GZO films by the pulsed laser deposition (PLD) method [8, 9]. The PLD-CeO_2/IBAD-GZO template is better aligned than any other template system examined so far. Furthermore, the CeO_2/GZO template system, more than 100 m long, has been able to be formed on non-textured alloy tape [10, 11]. Therefore, this template system is one of the most promising candidates for a buffer layer to achieve long YBCO films with high J_c on metal tape.

To prepare practical YBCO films with a high critical current (I_c) on metal tape with the textured CeO_2/GZO buffer layer, several methods have been applied, i.e., pulsed-laser deposition (PLD), metal organic chemical vapor deposition (MOCVD), electron beam (EB) and metal organic deposition (MOD). In particular, PLD can fabricate long YBCO films obtaining both J_c values of more than 1 MA/cm^2 and I_c values of more than 100 A on Hastelloy tape of 10 mm wide with buffered CeO_2/GZO multilayer [11–14]. In addition, using the PLD, continuous coated conductors more than 100 m long have been already produced [11, 12]. However, as the YBCO films prepared using PLD become thicker, more than 1 μm, the J_c values of the film decrease and the I_c values do not increase as much.

In this study, we characterize the nanostructures of PLD-YBCO films on Hastelloy with biaxially textured CeO_2/GZO multilayer using transmission electron microscopy (TEM) to investigate the relationships between the superconductive properties and the nanostructures. Local structures known to be strongly correlated with the superconductive properties of the YBCO films, in particular, the orientations and sizes of YBCO grains, defects in YBCO grains and secondary-phase oxides, were examined using selected-area diffraction patterns, dark-field image, high resolution image and elemental mapping using energy-dispersive X-ray spectroscopy (EDS).

2. Experimental procedures

2.1. PLD-YBCO

A GZO layer was deposited on a Hastelloy 10 mm wide using IBAD [6, 7], then a CeO_2 layer was formed on the GZO using PLD [9, 10]. Furthermore two thicknesses of the YBCO layer were fabricated by PLD on the buffered CeO_2/GZO multilayer. One was a 4-μm-thick YBCO layer with an I_c value of 173 A that was formed on a stationary substrate with referential deposition temperature of 760°C [13]. The other was formed using a reel-to-reel tape transferring system [14]. The YBCO layer was deposited 7 times in total. The substrate transferal rate was 10 m/h from the first to the sixth deposition, and then the last deposition was at 2 m/h. As the YBCO layer becomes thicker, referential deposition temperatures increase from 810 to 830°C. The total thickness of the YBCO film was 3 μm and the I_c value of the film was 293 A.

2.2. TEM specimen preparations and nanostructural characterization

Those YBCO layers were then thinned in a HITACHI FB-2100 focused ion beam (FIB) system at an accelerating voltage of 10–40 keV equipped with a micro-sampling system [15] for both the cross-sectional and plan-view TEM specimen. These TEM specimens were further milled in a Gatan Dual Ion Mill at an accelerating voltage of 2.0-1.5 keV to remove FIB damaged layers formed on the foil specimens [16, 17]. In the plan-view specimen using a micro-sampling, a thin plate 3 μm thick, 20 μm long and 30 μm deep spanning the region from the YBCO to the CeO_2 layer was picked up in FIB system, and then a thin-foil specimen was prepared using FIB milling. One edge of the foil specimen was located about 1 μm below the YBCO surface and the opposite edge about 0.2 μm into the CeO_2 layer from the YBCO/CeO_2 interface. Thus the plan-view specimen provides an efficient means of analyzing the nanostructural gradient from the substrate interface and crystal alignment of the various component layers [18].

The specimens were examined in a Topcon EM-002B TEM and a JEOL 4000FX TEM at an accelerating voltage of 200 and 400 keV, respectively.

3. Results and discussion

A cross-sectional low magnification electron micrograph of 4-μm-thick YBCO, with an I_c value of 173 A, on a Hastelloy with a CeO_2/GZO multilayer and selected-area diffraction patterns (SADPs), acquired from the marked area are shown in Fig. 1. The white broken line indicates the boundaries between *a*-and *c*-axes-oriented grains

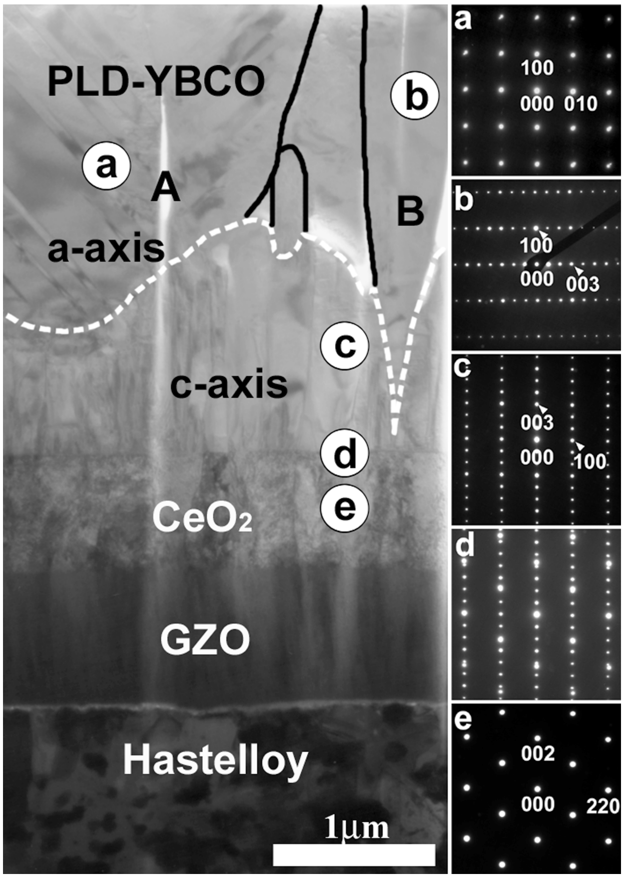

Figure 1 Cross-sectional low magnification electron micrograph of 4-μm-thick YBCO on a Hastelloy with a $CeO_2/Gd_2Zr_2O_7$ multilayer and SADPs. The white broken line indicates the boundaries between *a* - and *c*-axes-oriented grains and black lines between *a*-axis-oriented grains. Corresponding SADPs from the regions are marked (a)–(e).

and black lines indicate the boundaries between *a*-axis-oriented grains. The YBCO layer less than 1 μm thick is predominantly composed of *c*-axis-oriented grains and the layer further than 1 μm from the CeO_2 interface *a*-axis-oriented grains are more abundant. As shown in the micrograph, *a*-axis-oriented grains grow larger with the increase of the thickness of YBCO. According to the SADP shown in Fig. 1a, an *a*-axis-oriented grain indicated by "A" is projected along the ⟨001⟩ and the ⟨010⟩ is in the horizontal direction. According to the SADP shown in Fig. 1b, an *a*-axis-oriented grain (labeled as "B") is projected along the ⟨010⟩ and the ⟨001⟩ is parallel to the interface. Since the width of grain "A" is larger than that of the grain "B", the grain growth rate along the *a*- or *b*-axes seems to be higher than along the *c*-axis. Based on the SADP shown in Fig. 1d, the orientation relationships between YBCO and CeO_2 were found to be; (001)YBCO//(001)CeO_2 and (100)YBCO//(110) CeO_2.

Fig. 2 shows a dark-field image of YBCO on the CeO_2 using the (006) reflection of YBCO. The broken line also indicates the boundaries between *a*- and *c*-axes-oriented grains. Since many screw dislocations perpendicular to the CeO_2 interface are present in the *c*-axis-oriented grains, the grains are considered to grow spirally. These dislocations disappear under the $\vec{g} = 100$ and the $\vec{g} = 310$ YBCO conditions. Some large *c*-axis-oriented grains grow throughout the YBCO layer and an *a*-axis-oriented grain seems to nucleate on the CeO_2 interface from its shape, as shown in Fig. 3. In addition, many gaps or pores, which are not caused by the FIB milling, are found between YBCO grains. Using FIB milling, it is possible to prepare a thin-foil specimen while retaining original cracks [19] and pores [20–22].

Fig. 4 shows the results of the EDS elemental mapping for (a) Y, (b) Ba, (c) Cu (d) O and (e) a TEM image of the mapped region. The broken lines in Fig. 4e also indicate the boundaries between *a*- and *c*-axes-oriented grains. Bright contrast regions in Fig. 4a and c indicate Y_2O_3 and copper oxides, respectively. These secondary-phase oxides are formed at the boundaries between the *a*- and *c*-axes-oriented grains.

Fig. 5 shows a cross-sectional dark-field image of the 3-μm-thick YBCO layer with an I_c value of 293 A using the (006) reflection of YBCO. The broken lines also indicate the boundaries between *a*- and *c*-axes-oriented grains. In the YBCO layer composed of *c*-axis-oriented grains, a layer structure corresponding to the multi-deposition process is clearly observed, and arrows indicate the boundaries between each deposited layer. The thickness of each deposited layer from the first to the sixth deposition can be seen to be uniform. In addition, enormous stacking faults are observed in the each deposition layer. Since screw dislocations in *c*-axis-oriented grains penetrate each layer, formation of each layer is strongly correlated to the orientation and the local structure of the underlying layer. However, a small number of narrow gaps, a few dozen nanometers wide, were formed at the boundary between *c*-axis-oriented grains in the cross-sectional specimen [23]. In addition, a small amount of copper oxides were found at the bottom of the gaps [23].

By increasing the referential substrate temperature compared to that of the 4-μm-thick YBCO layer, the nucleation of *a*-axis-oriented grains on the CeO_2 interface in this specimen seemed to be suppressed. However, an *a*-axis-oriented grain on the right hand side of Fig. 5 is considered to have nucleated on the 4th YBCO deposition layer. Nucleation points of *a*-axis-oriented grains are considered to be grain boundaries, spiral steps of the *c*-axis-oriented grains, or a small amount of surface roughness caused by the PLD process. However, note that each deposited YBCO layer as well as the CeO_2 layer [24] should have those surface defects. Therefore, in this PLD process, the nucleation of *a*-axis-oriented grains is considered to be strongly affected by the deposition temperature. The deposition temperature on the YBCO surface would be lower than the referential substrate temperature due

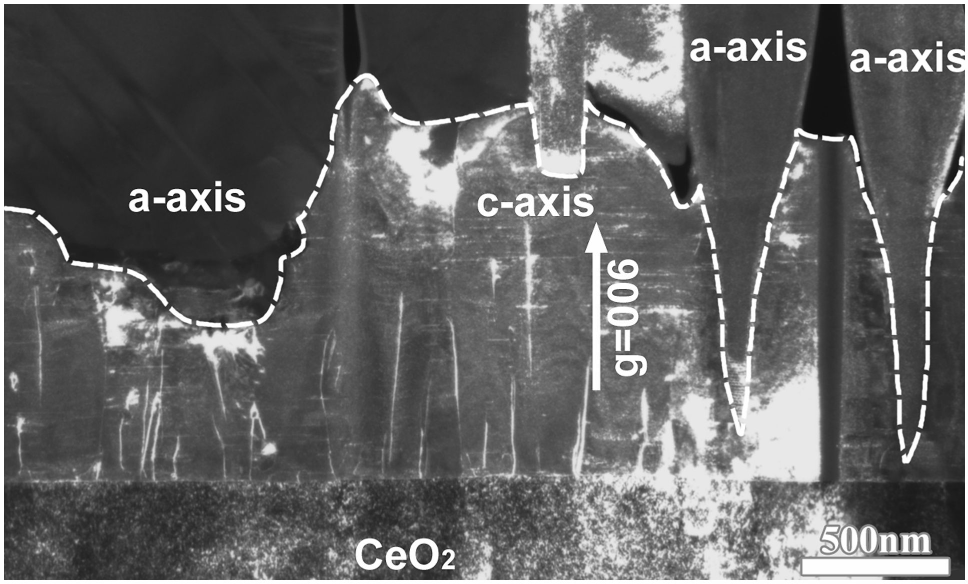

Figure 2 Dark-field image of a YBCO film on the CeO_2 using the (006) reflection of YBCO.

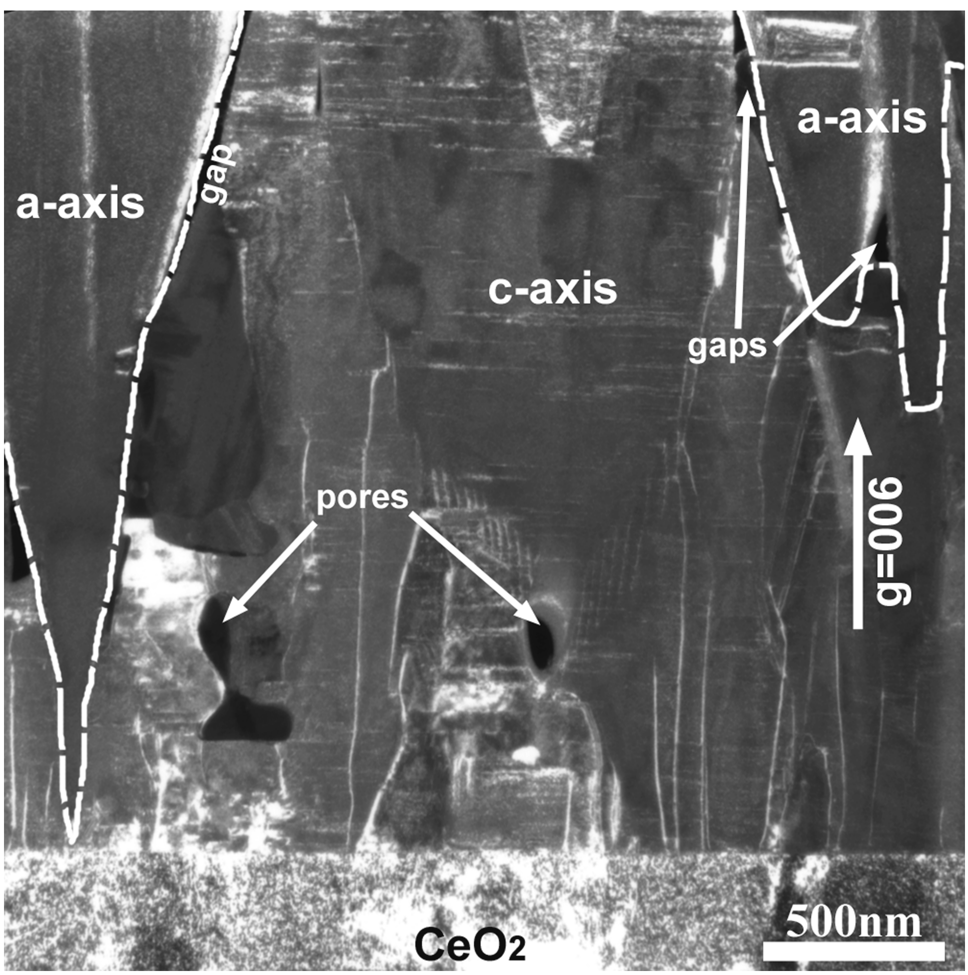

Figure 3 Dark-field image of YBCO grains with a *c*-axis-oriented grain from the CeO_2 interface to the surface of the YBCO. An *a*-axis-oriented grain is likely to nucleate on the CeO_2 interface on the left-hand side.

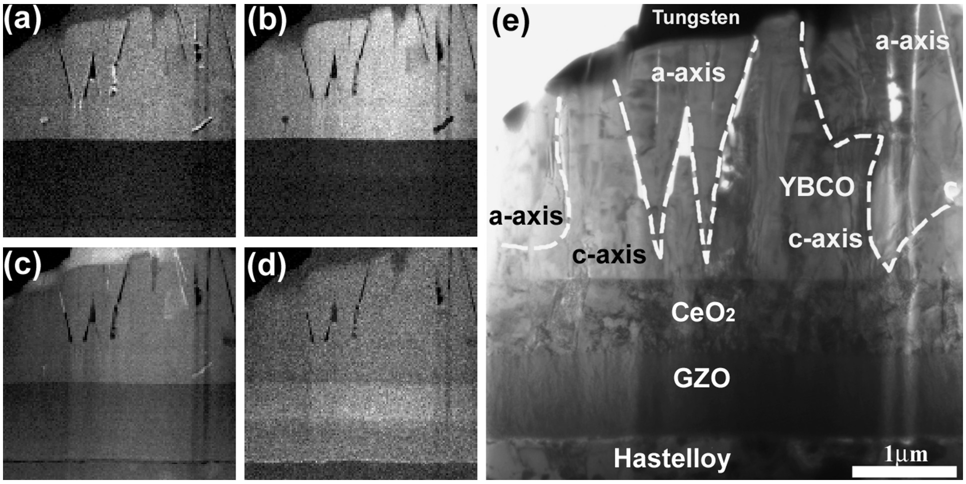

Figure 4 The EDS elemental maps for (a) Y, (b) Ba, (c) Cu (d) O and (e) TEM image of the mapped region.

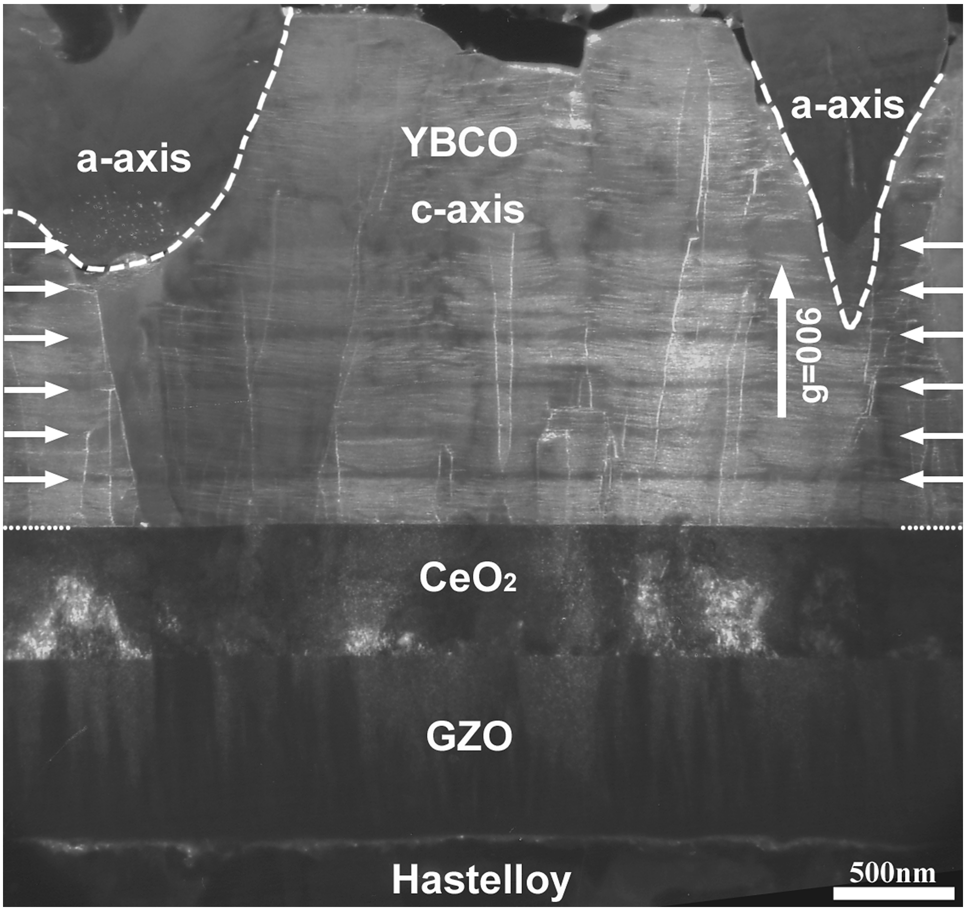

Figure 5 Cross-sectional dark-field image of 3-μm-thick YBCO on a Hastelloy with CeO_2/GZO multilayer using the (006) reflection of YBCO.

to the thermal conductivities of the YBCO or radiational cooling from the YBCO surface. For these reasons, it is important to determine the optimum referential substrate temperatures of the thickness of YBCO for each deposition process. Furthermore, since it is easy to control substrate temperature for each thickness of YBCO using a reel-to-reel tape transferring system, multi-deposition processes are thought to be best suited for the production of long YBCO-coated conductor with high I_c values.

Fig. 6 shows a plan-view image of 3-μm-thick YBCO/CeO_2. The white arrows indicates the interface between the YBCO and the CeO_2. As shown in the cross-

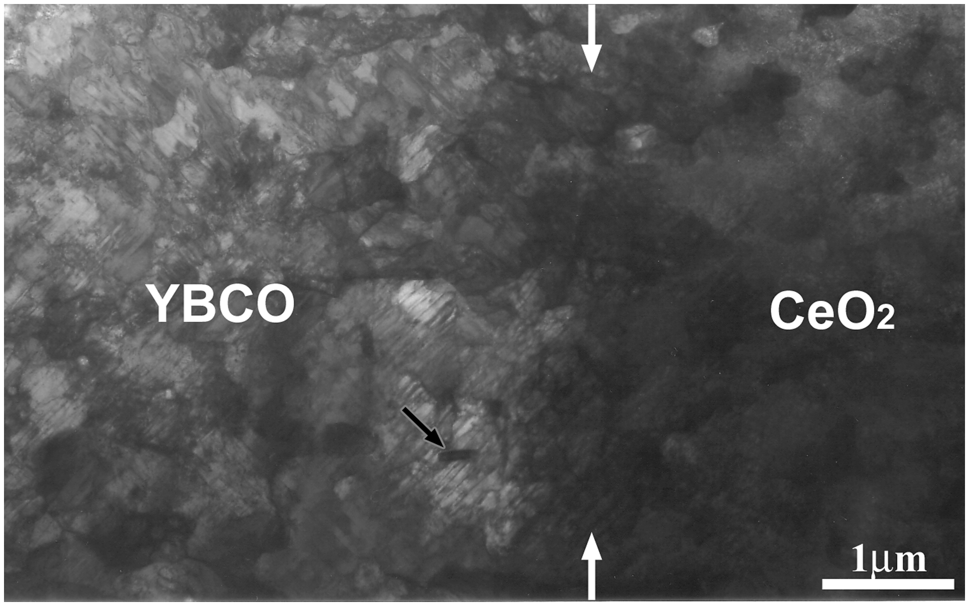

Figure 6 Low magnification plan-view image of 3-μm-thick YBCO/CeO_2.

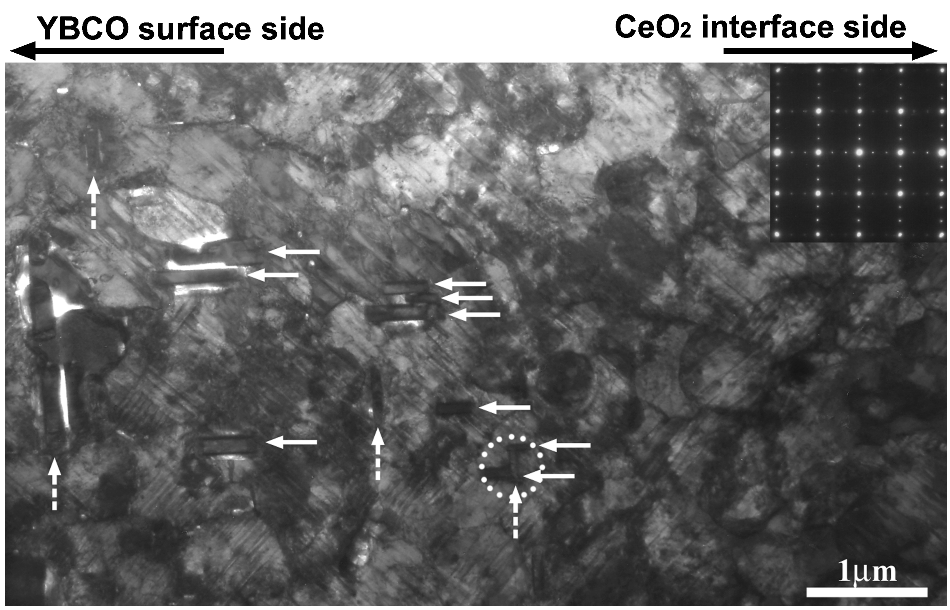

Figure 7 Low magnification plan-view image of 3-μm-thick YBCO beyond about 2 μm from the CeO_2 interface. Inset is a SADP corresponding to the region indicated by dotted circle in the micrograph.

sectional specimen, the YBCO layer near the CeO_2 is predominantly composed of c-axis-oriented grains, which have many twin boundaries. Some twin boundaries penetrate the grain boundaries of c-axis-oriented grains. Such grain boundaries are considered to be small tilt angle grain boundaries. However, a small number of a-axis-oriented grains, which have not been found in the cross-sectional specimen [23] (indicated by a black arrow) is observed near the CeO_2 interface. Fig. 7 shows a plan-view image of 3-μm-thick YBCO further than about 2 μm from the CeO_2 interface and the inset a SADP corresponding to the region indicated by the dotted circle in the micrograph. Many a-axis-oriented grains indicated by broken and unbroken arrows in Fig. 7 are observed. According to the SADP, the $\{001\}$ planes of a-axis-oriented grains indicated by the broken arrows are perpendicular to those of the unbroken arrows. In addition, as observed in the cross-sectional specimen, the grain size of a-axis-oriented grains gradually becomes larger with the increasing thickness of the YBCO layer. In addition, gaps are found between a- and c-axes-oriented grains.

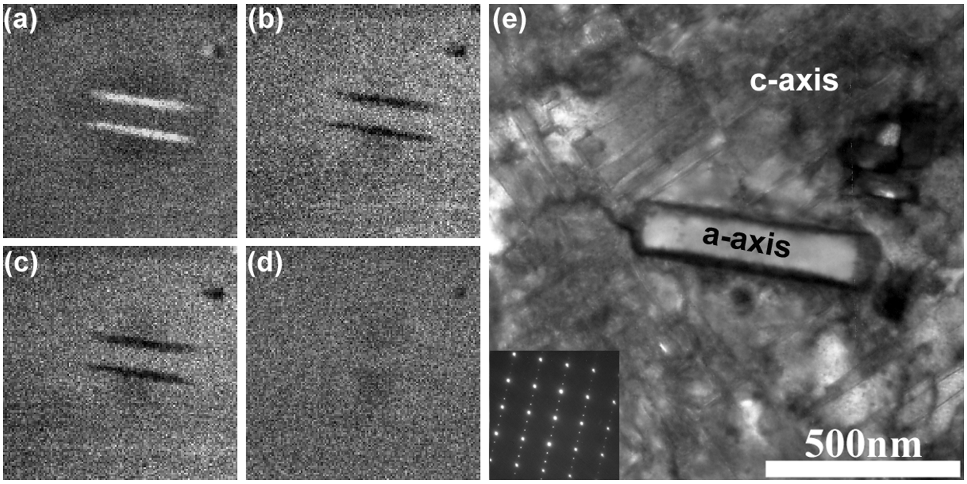

Figure 8 The EDS elemental maps for (a) Y, (b) Ba, (c) Cu (d) O and (e) TEM image of the mapped region. Inset is a SADP from the *a* - and *c*-axes-oriented grains.

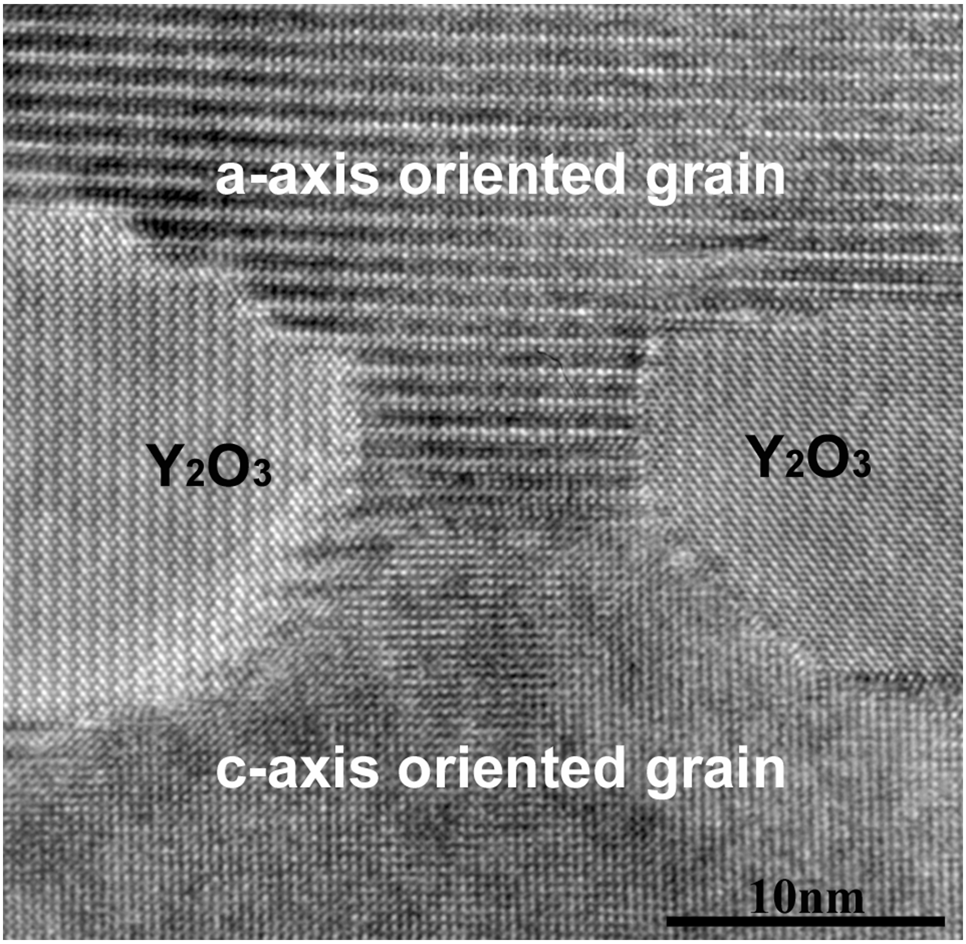

Figure 9 Plan-view high-resolution image of the boundary between *a*- and *c*-axes-oriented grains.

Fig. 8 shows the EDS elemental maps for (a) Y, (b) Ba, (c) Cu, (d) O and (e) a TEM image of the mapped region and, with a SADP inset from *a*- and *c*-axes-oriented grains. In the Y-map in Fig. 8 a, bright contrast reveals Y_2O_3 grains, which have not been found in the cross-sectional specimen [23], between *a*- and *c*-axes-oriented grains. According to the result of the Y map in (a) and the SADP in (e), the Y_2O_3 grains are formed between the

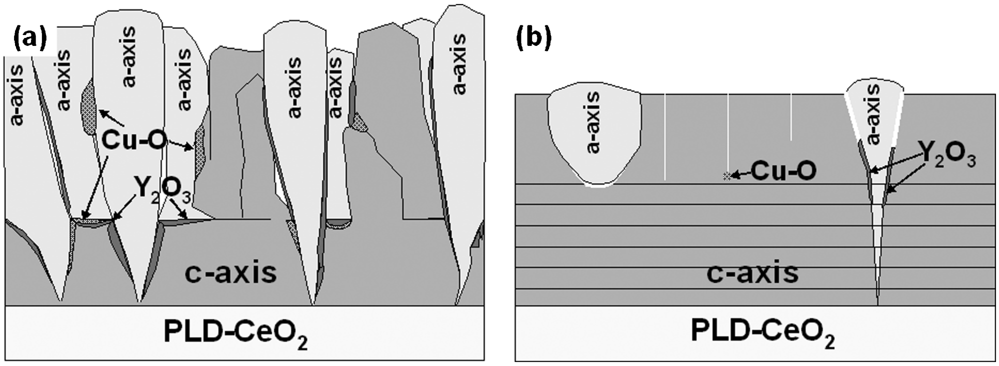

Figure 10 Schematic illustrations of the PLD-YBCO films on CeO_2 (a) 4-μm-thick YBCO film with an I_c value of 173 A and (b) 3-μm-thick YBCO film with that of 293 A.

{001} plane of the *a*-axis-oriented grain and the {100} or {010} plane of the *c*-axis-oriented grain.

Fig. 9 shows a plan-view high-resolution image of the boundary. Since the directions of lattice fringes in both the Y_2O_3 grains are almost the same, the orientation relationships between YBCO and Y_2O_3 are as follows; (001)YBCO//(001)Y_2O_3 and (100)YBCO//(110)Y_2O_3.

Fig. 10 shows cross-sectional schematic illustrations of the PLD-YBCO films on CeO_2 (a) 4-μm-thick YBCO and (b) 3-μm-thick YBCO. As the YBCO films become thicker, *a*-axis-oriented grains grow larger. It seems that the growth rates along the *a*- or *b*-axes are higher than those along the *c*-axis in *a*-axis-oriented grains. In 4-μm-thick YBCO, a large number of *a*-axis-oriented grains is considered to nucleate at the CeO_2 interface. Y_2O_3 and copper oxides are formed at the boundaries between the *a*- and *c*-axes-oriented grains. In addition, many gaps and pores are found between YBCO grains. In 3-μm-thick YBCO, the number of nucleation of *a*-axis-oriented grains on the CeO_2 is much smaller than that of the 4-μm-thick YBCO owing to an increase in the referential substrate temperature. However, many *a*-axis-oriented grains nucleate after several YBCO depositions, and then Y_2O_3 grains and porous structures are also formed between YBCO grains. *a*-axis-oriented grain growth and the formation of impurity oxides and porous structures between YBCO grains are considered to cause the reduction of the J_c values. Therefore, it is necessary to determine the optimum process conditions to suppress the nucleation of *a*-axis-oriented grains.

4. Conclusions

We prepared cross-sectional and plan-view specimens, which provided an efficient means of analyzing the nanostructural gradient and crystal alignment of component layers, for two thicknesses of PLD-YBCO films on Hastelloy with a textured CeO_2/GZO multilayer. One is 4-μm-thick YBCO with an I_c value of 173 A, and the other is 3-μm-thick film with an I_c value of 293 A. Then, the nanostructural characterization of these specimens was achieved by TEM. The conclusions are as follows;

1. The YBCO films were predominantly composed of *c*-axis-oriented grains near the CeO_2 interface. Since many screw dislocations perpendicular to the CeO_2 interface were observed in *c*-axis-oriented grains, the grains were considered to grow spirally.
2. We found *a*-axis-oriented grains nucleated in the YBCO films and those grains grow larger with the increase of the thickness of the YBCO films.
3. Y_2O_3, copper oxides and porous structures were formed at the boundaries between *a*- and *c*-axes-oriented grains. Y_2O_3 grains were formed between the {001} plane of an *a*-axis-oriented grain and the {100} or {010} plane of a *c*-axis-oriented grain. The orientation relationships between YBCO and Y_2O_3 were determined as follows; (001)YBCO//(001)Y_2O_3 and (100)YBCO//(110)Y_2O_3.
4. Since *a*-axis-oriented grain growth is considered to reduce the J_c values of the YBCO films, it is important to optimize the process conditions that suppress the nucleation of the *a*-axis-oriented grains in order to produce practical YBCO films with a high I_c values. The YBCO deposition temperature is one of most important process parameter to achieve high quality YBCO films.

Acknowledgment

This work was supported by the New Energy and Industrial Technology Development Organization (NEDO) as the Collaborative Research and Development of Fundamental Technologies for Superconductivity Applications.

References

1. Y. IIJIMA, N. TANABE, Y. IKENOA and O. KOHNOA, *Physica C* **185** (1991) 1959.
2. Y. IIJIMA, N. TANABE, O. KOHNO and Y. IKENO, *Appl. Phys. Lett.* **60** (1992) 769.
3. J. DZICK, J. HOFFMANN, S. SIEVERS, L. O. KAUSTCHOR, H. C. FREYHARDT, *Physica C* **372–376** (2002) 723.
4. Y. IIJIMA, K. KAKIMOTO, T. SAITOH, T. KATOH and T. HIRAYAMA, *J. Jpn. Inst. Metals* **66** (2002) 528.
5. *Idem., Physica C* **378–381** (2002) 960.
6. S. MIYATA, T. WATANABE, T. MUROGA, H. IWAI, Y. YAMADA, Y. SHIOHARA, T. KATO and T. HIRAYAMA, *J. Jpn. Inst. Metals* **68** (2004), 723.

7. S. MIYATA, T. WATANABE, T. MUROGA, H. IWAI, Y. YAMADA and Y. SHIOHARA, *Physica C* **412–414** (2004) 824.
8. T. MUROGA, T. ARAKI, T. NIWA, Y. IIJIMA, T. SAITOH, I. HIRABAYASHI, Y. YAMADA and Y. SHIOHARA, *IEEE Trans. Appl. Supercond.* **13** (2002) 2532.
9. T. MUROGA, T. WATANABE, S. MIYATA, H. IWAI, Y. YAMADA, T. IZUMI, Y. SHIOHARA, T. KATO, H. SASAKI, Y. SUGAWARA and T. HIRAYAMA, *Physica C* **412–414** (2004) 807.
10. T. MUROGA, S. MIYATA, T. WATANABE, A. IBI, Y. YAMADA, T. IZUMI, Y. SHIOHARA, T. KATO and T. HIRAYAMA, *J. Cryo. Soc. Jpn.* **39** (2004) 529.
11. Y. IIJIMA, K. KAKIMOTO, Y. SUTOH, S. AJIMURA and T. SAITOH, *Physica C* **412–414** (2004) 801.
12. *Idem., Supercnd. Sci. Technol.* **17** (2004) 264.
13. H. IWAI, T. MUROGA, T. WATANABE, S. MIYATA, Y. YAMADA, Y. SHIOHARA, T. KATO and T. HIRAYAMA, *ibid.* **17** (2004) 496.
14. T. WATANABE, H. IWAI, A. IBI, T. MUROGA, S. MIYATA, Y. YAMADA, Y. SHIOHARA, T. KATO and T. HIRAYAMA, *IEEE Trans. Appl. Supercond.* submitted for publication.
15. T. OHNISHI, H. KOIKE, T. ISHITANI, S. TOMIMATSU, K. UMEMURA and T. KAMINO, in Proc. of the 25th Inter. Symp. for Test. and Failure Analys. (Santa Clara, California, 1999) p. 449.
16. T. MATSUDA, *Materia Jpn.* **42** (2003) 916.
17. H. SASAKI, T. MATSUDA, T. KATO, T. MUROGA, Y. IIJIMA, T. SAITOH, F. IWASE, Y. YAMADA, T. IZUMI, Y. SHIOHARA and T. HIRAYAMA, *J. Electron Microsc.* **53** (2004) 497.
18. T. KATO, T. MUROGA, Y. IIJIMA, T. SAITOH, Y. YAMADA, T. IZUMI, Y. SHIOHARA, T. HIRAYAMA and Y. IKUHARA, *ibid.* **53** (2004) 501.
19. H. SAKA and S. ABE, *ibid.* **46** (2004) 45.
20. T. KATO, Y. SASAKI, K. OSADA, T. HIRAYAMA and H. SAKA, *Surf. Interface Anal.* **31** (2001) 409.
21. H. MUCHA, T. KATO, S. ARAI, H. SAKA, K. KURODA and B. WIELAGE, *J. Electr. Microsc.* **54** (2005) 43.
22. T. KATO, K. MATSUMOTO, H. MATSUBARA, Y. ISHIWATA, H. SAKA, T. HIRAYAMA and Y. IKUHARA, *Surf. Coat. Technol.* **194** (2005) 16.
23. T. KATO, H. SASAKI, H. IWAI, A. IBI, N. KASHIMA, T. NIWA, T. MUROGA, S. MIYATA, T. WATANABE, Y. IIJIMA, K. KAKIMOTO, Y. SUTOH, Y. YAMADA, S. NAGAYA, T. SAITOH·, T. IZUMI, Y. SASAKI, T. HIRAYAMA, Y. SHIOHARA and Y. IKUHARA, submitted to *Physica C*, in press.
24. T. KATO, T. MUROGA, Y. IIJIMA, T. SAITOH, T. HIRAYAMA, I. HIRABAYASHI, Y. YAMADA, T. IZUMI, Y. SHIOHARA and Y. IKUHARA, *Physica C* **412–414** (2004) 813.